Experimental investigation of reinforcement strategies for concrete extrusion 3D printed beams

Author(s):
Gebhard, Lukas; Mata Falcón, Jaime; Anton, Ana; Dillenburger, Benjamin; Kaufmann, Walter

Publication date:
2020-08

Permanent link:
https://doi.org/10.3929/ethz-b-000444960

Experimental investigation of reinforcement strategies for concrete extrusion 3D printed beams

Lukas Gebhard[1,*], Jaime Mata-Falcón[1], Ana Anton[2], Benjamin Dillenburger[2] and Walter Kaufmann[1]

[1] Institute of Structural Engineering, Department of Civil, Environmental and Geomatic Engineering, ETH Zurich, Switzerland
[2] Digital Building Technologies, Department of Architecture, ETH Zurich, Switzerland
** Corresponding author*
gebhard@ibk.baug.ethz.ch

Abstract
This study investigates the structural behaviour of different reinforcement concepts for extrusion-based 3D concrete printed beams. As longitudinal reinforcement, unbonded post-tensioning and passive bonded reinforcement are explored. As shear reinforcement, fibres and cables placed between the layers of concrete are analysed. The results of four-point bending tests show that unbonded reinforcement leads to highly brittle failure without a proper activation of the shear reinforcement. The beams with conventional bonded reinforcement behave monolithically, with little influence of the concrete layering. Cables, as well as fibres, increase the shear resistance significantly. While cables have higher efficiency, fibres lead to finer and more closely spaced cracks.

1 Introduction

New digital fabrication with concrete (DFC) technologies open up many new possibilities for the construction industry [1]. Among these technologies, Concrete Extrusion 3D Printing (CE3DP) is the most known process, where a robotic system can add concrete in successive layers to reconstruct a digital object. Due to extensive research efforts in this field, technological and material challenges have been overcome to a large extent. However, there is still a lack of consistent reinforcement strategies, which are essential for this technology to have a relevant impact on the construction market. These reinforcement strategies should result in a ductile behaviour of the structural elements, to allow for a plasticity-based design philosophy similar to the actual design of conventionally built structures. This study investigates two reinforcement approaches for the longitudinal reinforcement and two shear reinforcement strategies for 3D printed beams. The experimental campaign consists of four-point bending tests of the beams, which are tracked by digital image correlation (DIC).

2 Reinforcement strategies

Currently, there is a vast interest in the development of reinforcement strategies for DFC. The current state of the art is summarised in [2]. One of the main challenges of these reinforcement strategies is to provide a ductile structural system without, at the same time, hindering the potentials of digital fabrication. Therefore, the authors developed a novel reinforcement strategy where fibres are placed between layers of concrete in an aligned and controlled manner [3, 4] (Fig. 1). Since previous work showed that this reinforcement approach is not suitable as the main reinforcement, this reinforcement strategy is used to provide shear reinforcement. For comparison, steel cables are used as shear reinforcement, which is derived from previous work [5, 6]. For the longitudinal reinforcement, this study investigates the use of post-tensioning or conventional reinforcement, similar as in previous studies [7]. The objective of the combined reinforcement approach consists in activating the cables, as well as the fibres, as shear reinforcement, providing a post-cracking shear resistance once diagonal cracks develop, while the main tensile loads are carried by the longitudinal reinforcement.

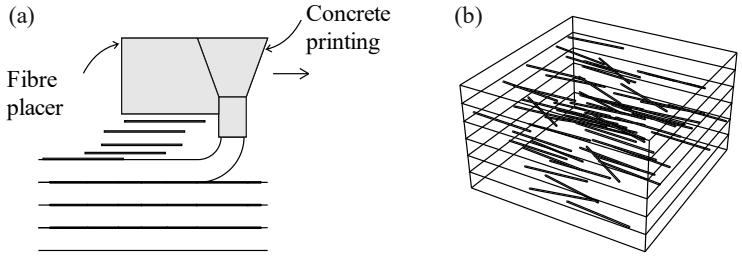

Fig. 1: Schematic sketch of the reinforcement concept for interlayer fibre reinforcement: (a) concrete layers printed by a nozzle with the continuous placement of fibres; (b) resultant layered concrete with aligned fibres in-between the layers [3].

3 Experimental campaign

3.1 Specimens and materials

Two series of beams with different longitudinal reinforcement were produced for this study (see the overview of samples in Table 1). The first series used unbonded post-tensioning (Series 01), and the second series used conventional bond reinforcement (Series 02). Series 01 only used fibres as shear reinforcement, while Series 02 explored fibres and cables as shear reinforcement. A reference beam without shear reinforcement was printed simultaneously to each beam with shear reinforcement. In total, Series 01 consisted of four beams (two with fibre reinforcement and two without) and Series 02 of five beams (one with cable reinforcement, two with fibre reinforcement and two with no shear reinforcement). The geometry of the samples is shown in Fig. 4. The beams from Series 01 had a nominal height (H) of 300 mm, a width (W) of 150 mm and a total length (L) of 1500 mm. The dimensions of Series 02 were slightly larger: H: 320 mm, W: 200 mm and L: 1720 mm. Due to the particularities of CE3DP, the actual printed width (WW, provided in Table 1) differed from the nominal values specified in Fig. 4.

The concrete used in this project was a fine-grained concrete with a maximum aggregate size of 2 mm. The average compressive strength for Series 01, measured at the same age of the tests, was 71.5 MPa (tested on eight cylinders 150x300 mm), and the tensile strength was 2.4 MPa (tested via

Table 1: Overview of samples: Average web width (WW), average prestressing stresses ($\sigma_{c,p.}$), shear reinforcement type (SR), nominal shear reinforcement ratio (ρ_{SR}) and age at testing (Age).

Beam Nr.	Series	Codification	Printing session	Glued	WW [mm]	$\sigma_{c,p}$ [MPa]	SR	ρ_{SR} [vol%]	Age [d]
111	01	B-111-NR	11	Yes	45	-9	-	-	28
112	01	B-112-F03	11	Yes	45	-9	Fibres	0.3	31
121	01	B-121-NR	12	Yes	50	-7.5	-	-	29
122	01	B-122-F03	12	Yes	50	-7.5	Fibres	0.3	29
211	02	B-211-NR	21	No	62	-	-	-	28
212	02	B-212-C01	21	No	61	-	Cables	0.1	28
221	02	B-221-NR	22	No	57	-	-	-	28
222	02	B-222-F03	22	No	58	-	Fibres	0.3	28
231	02	B-231-F06	23	Yes	63	-	Fibres	0.6	50

double punch tests on four cylinders 150x150 mm). The same tests were used to assess the compressive strength of Series 02, with 67.5 MPa compressive strength (tested on six cylinders) and 2.3 MPa tensile strength (tested on six cylinders). All tested samples were made from the extruded accelerated concrete. The longitudinal reinforcement for Series 01 consisted of two high strength threaded rods with a diameter of 24 mm (M24 10.9). For Series 02, the conventional passive reinforcement were two B500B steel bars with a diameter of 26 mm and threads at both ends (i.e. bartec technology [8]) to enable anchorage. The cable reinforcement was a high strength steel cable composed of 19 wires, type 1x19 [9], with a nominal cable diameter of 1 mm and an average tensile failure load of 1.3 kN (measured on ten samples). The used fibres for both series are end hooked steel fibres of the type Dramix 3D 65/35 [10].

3.2 Production of the beams

3.2.1 Concrete extrusion 3D printing

The beams were produced by a set-on-demand [11] CE3DP system in the Robotic Fabrication Laboratory of ETH Zürich (Fig. 2.a). The system used two main components: Portland Cement based mortar (PC) and Calcium Aluminate Cement paste accelerator (CAC), which were actively intermixed inside the custom extruder-tool [12]. After extrusion, concrete starts hardening, thus enabling a vertical building rate of up to 3 meters per hour. Two progressive cavity pumps delivered PC and CAC into the extruder-tool, which was mounted on the 6th axis of the robotic manipulator (Fig. 2.b). The entire kinematic system consisted of an ABB 4600 robotic manipulator mounted on a 3-axis Güdel Gantry. Both pumps were manually supplied with materials and digitally controlled through the robotic interface. Motion commands were loaded as procedures into the robotic controller and executed in manual mode to allow human presence in the immediate proximity of the robot.

The beams were always printed vertically in pairs: one containing shear reinforcement and a reference one without reinforcement (Fig. 3.d). The nominal geometry of the beam was sliced with horizontal planes spaced at the layer-height (5 mm). The print path was designed to fabricate the shear reinforced beam and the reference one in a single printing session (i.e. four beam parts for Series 01 which were afterwards glued together into two beams and two full beams for Series 02). The transition from one beam to the next was made in one of the top corners of each section. The print path for Series 02 is shown in Fig. 3.d. The concrete filament width was controlled with the speed of the robot (e.g. for Series 02 a 25 mm layer-width was printed at a speed of 160 mm/s). The cross-section of Series 01 was produced with a single print path, while two adjoining print paths produced the cross-section of Series 02. The technology allows producing hollow sections, which in this study were used for inserting longitudinal reinforcement or left hollow.

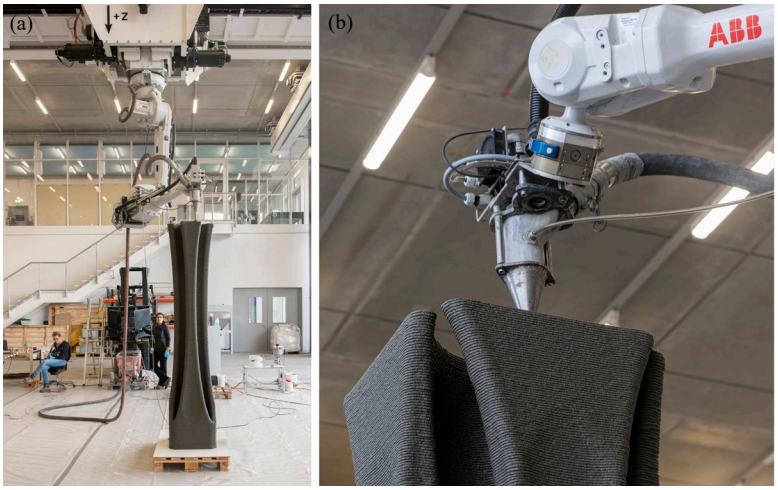

Fig. 2: CE3DP system developed at ETH Zurich, used to fabricate the beams: (a) kinematic system and progressive cavity pumps; (b) extruder tool [Photos by Axel Crettenand].

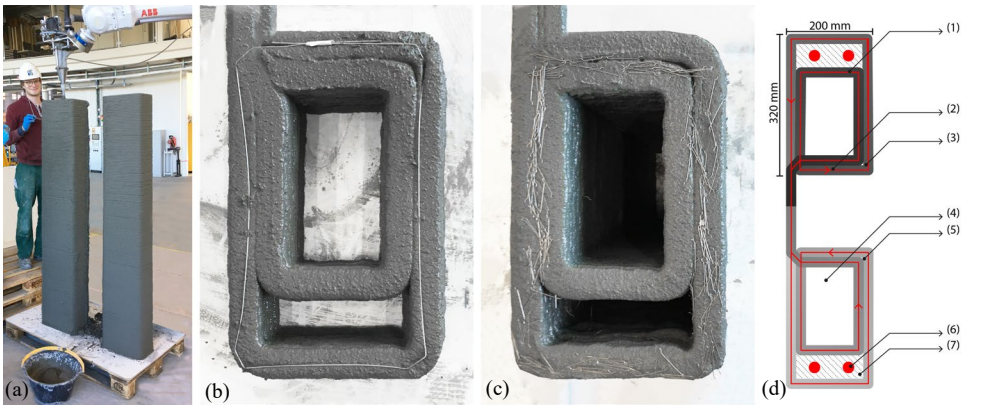

Fig. 3: Production of beams, Series 02: (a) Vertical printing of two beams; (b) cross-section with cable reinforcement; (c) cross-section with fibre reinforcement; (d) print path ((1) filament width 25 mm with gradient colour indicating the material deposition sequence, (2) direction of the print path, (3) beam without shear reinforcement, (4) hollow core of the beam, (5) shear-reinforced beam, (6) post-installed reinforcement, (7) cast concrete).

3.2.2 Placing of shear reinforcement

The two types of shear reinforcement (i.e. cables and fibres) were placed manually in-between the layers of concrete during printing for every second layer. The cables were pre-bent to fit the printing path and had an overlap in the upper flange of the beam of about 10 cm (Fig. 3.b). The total fibre content was determined with respect to the nominal concrete volume of each beam and afterwards subdivided for each interlayer. Due to the variations in the print path width, the final volume fractions deviated from the nominal ones (see Table 1). The fibres were first detached from each other by washing, then weighed to the correct amount, then placed on foils on top of magnetic strips and laid onto the concrete layer. After placing, first, the magnetic strip and afterwards, the foil was removed, leaving only the fibres in an aligned manner on top of the concrete (Fig. 3.c). For Series 01, fibres were only placed in the webs of the beams, whereas for Series 02, fibres and cables were placed all around the cross-section.

3.2.3 Preparation for testing

After hardening, the beam ends were cut to obtain flat surfaces for glueing and for placing the reinforcement anchor plates. For Series 01 two identical pieces were glued together with epoxy to reach the final length. The specimens of Series 02 were printed as one beam, except for Beam 231 which was also glued, assembling one piece without fibres and one with fibres. The side without fibres was externally shear reinforced to provoke failure in the fibre reinforced part. Since the printed surface presented some irregularities, local mortar beds were applied in the load induction and support areas in all cases. Next, the longitudinal reinforcement was placed in the void of the cross-section. As anchorage, a steel plate was used on both ends of the beams. For Series 02, to ensure bond between the reinforcement bars and the surrounding concrete, the void was grouted afterwards with the same concrete mixture used for printing, however, without the use of the accelerator. Series 01 used two prestressing bars for the post-tensioning. Each bar was composed of two rods connected by means of a mechanical anchor at midspan. For Beams 111 and 112, the prestressing force was applied to have a constant compression of 9 MPa across the entire cross-section. For beams 121 and 122, the prestressing was adjusted to a compressive stress of 12 MPa at the bottom and 3 MPa on top. Prestressing forces were controlled by load-cells (see Section 3.3). Before testing, a thin layer of gypsum was applied on one side of the 3D printed concrete to obtain a smooth surface for the application of a speckle pattern for the DIC measurement.

3.3 Test setup and protocol

After preparation, the beams were placed in a loading frame. The loading configuration is shown in Fig. 4. The load was applied by means of a manual hydraulic pump. Series 01 was instrumented with

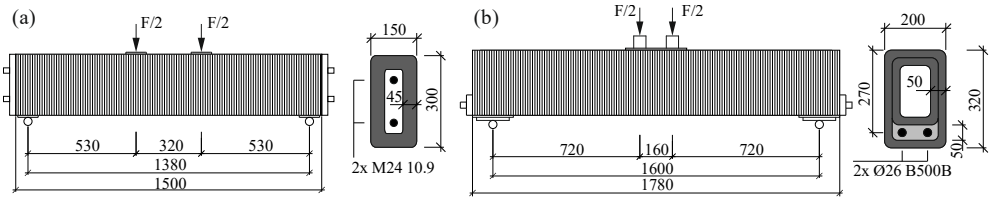

Fig. 4: Test setup and geometry of the specimens (dimensions in mm; cross-sections scaled by a factor of 1.5 compared to the test setup): (a) Series 01; (b) Series 02.

one load cell on each post-tensioning bar and one on each loading cylinder. For Series 02 the load was measured for the single loading cylinder and one of the supports. For both series, the entire surface was tracked with digital image correlation [13–15]. This allows tracking the entire displacement field including the beam's deflections at midspan, which are reported in the following. It is assumed that the thin gypsum layer follows the deformations of the concrete surface it was applied to. The crack pattern was computed from the DIC information by using the Automated Crack Detection and Measurement procedure [16].

4 Results

4.1 Series 01: unbonded post-tensioning reinforcement

Fig. 5 summarises the load-deformation curves for Series 01. Generally, all beams behaved similarly. In the first phase, all beams remained uncracked. After crack formation, the stiffness decreased, and the force could be further increased until the ultimate load was reached. The beam set of Beam 121 and 122 reached a higher ultimate load compared to the other set. This increase might have been due to the preferable initial prestressing state with -12 MPa at the bottom and -3 MPa on top and the larger web thickness. Beam 111 reached the lowest ultimate load and deformation. Both beams with fibre reinforcement showed mainly bending cracks, while the unreinforced beams also displayed significant cracking in the longitudinal direction. For Beam 111, this was likely due to large out of plane deformations. For Beam 121 these longitudinal cracks formed in the area of connection between the two prestressing rods, which might have introduced some lateral pressure into the web. No initiation of shear cracks could be observed in any of the tests. However, all beams experienced longitudinal cracks inside the upper flange (only visible from the top), indicating the necessity of also reinforcing the flanges. For both beam sets, the beam with fibre reinforcement reached a higher ultimate load than the reference specimens without shear reinforcement. All specimens failed in a brittle manner. However, while the beams without shear reinforcement failed in a highly explosive manner, the beams with fibres in the webs failed locally in the compression zone keeping the overall structure intact.

The lack of shear failures and shear cracks for specimens with unbonded longitudinal reinforcement was already reported by Leonhardt and Walther in 1962 [17]. In that study, it was stated that no shear failures could be reached without bond in the longitudinal reinforcement since the load was carried by strut-and tie action. In this way, high forces can be resisted if the tensile force in the reinforcement can be properly anchored. However, for non-symmetrical loading, this system is problematic and could lead to sudden catastrophic failure, since no ductility can be provided. The influence of having bonded longitudinal reinforcement is assessed in a second test series, whose results are presented in the following.

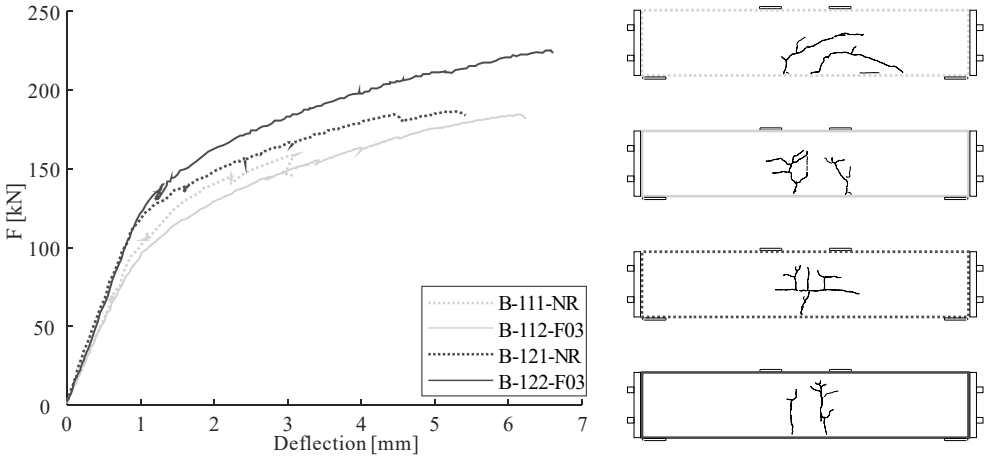

Fig. 5: Load deformation curves and crack patterns right before failure for Series 01.

4.2 Series 02: bonded passive reinforcement

Fig. 6 shows the load-deformation curves and the crack patterns for Series 02. For all beams, shear cracks were observed, and the failure was due to shear (diagonal tension). The two unreinforced beams (dotted lines) showed the lowest ultimate load. In both beams, shear cracks initiated at around 100 kN. While Beam 221 failed upon the formation of shear cracks, in Beam 211 the load could further be increased. This increase was likely due to interlock of the shear crack and the wider web thickness. In both cases, sudden load drops occurred after the first shear cracks formed, and the final failure was highly brittle.

The cable reinforced beam (Beam 212) formed the first shear cracks at a similar load as its reference beam without shear reinforcement, but the load could afterwards be increased to close to 300 kN. At the ultimate load, almost all cables over the length of the dominant shear crack ruptured simultaneously, leading to brittle failure. The rupture of the cables indicates that bond was sufficient to anchor the cables. The beam with 0.3% of fibres (Beam 222) could not reach the same ultimate load as Beam 212, even though the mechanical reinforcement content of the two beams was designed to be similar. After the formation of the first shear cracks, the aligned fibres were able to bridge the crack until they were pulled out at a maximum load of about 220 kN. For Beam 231 the fibre content was doubled. Consequently, the ultimate load could be significantly increased. However, the increase in ultimate load was not proportional to the increase in fibre content. This might have been due to the higher amount of fibres in the same layer resulting in a lower bond or to the presence of additional resistance mechanisms different than the fibre contribution. In both beams with fibre reinforcement, the fibres started to pull out, and at a certain point, the process became unstable, resulting in brittle failure.

As seen in the crack patterns, all specimens developed shear cracks. However, for the beams with fibre reinforcement, the crack spacing was smaller than for the cable reinforced beam. This could be beneficial for applications in which the service limit state is decisive. If the load-bearing capacity is decisive, the cables have higher efficiency, given that they are continuous and can be fully anchored. Contrary to previous work on metal cables as reinforcement, no issues with cable slipping were encountered in the present study [5].

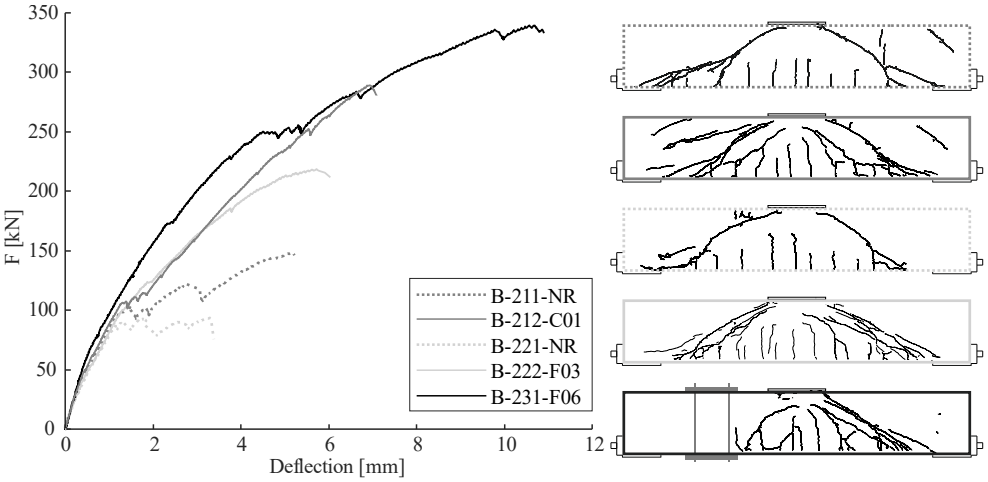

Fig. 6: Load deformation curves and crack patterns right before failure for Series 02.

5 Conclusions

This study presented two different reinforcement strategies for longitudinal reinforcement and two approaches to include shear reinforcement between the layers of printed concrete. The use of prestressing bars without bond as the main reinforcement led, for the studied load configuration, to high ultimate loads. However, since there was no bond between the reinforcement and the concrete, no shear cracks could be initiated, all the deformation was localised in a few bending cracks, and the failure was brittle. In some digitally fabricated structures, this approach is already used, since it allows installing the reinforcement after concrete production and, after prestressing, keeping the concrete in a state of pure compression. When using this reinforcing strategy, the concrete around the post-tensioning bars should be reinforced to avoid a catastrophic collapse in case the concrete is damaged.

In the case of conventional bonded reinforcement as longitudinal reinforcement, the structure behaved monolithically with the reinforcement. This allowed the formation of multiple bending cracks, with smaller crack openings and the formation of shear cracks, which can activate the shear reinforcement if present. This results in a more predictable system with smaller crack openings. However, the use of conventional reinforcement does hinder the geometric freedom of digital fabrication. A higher degree of geometric flexibility might be achieved when using flexible post-tensioning cables, which can be injected afterwards, as explored in this study. Whenever non-straight post-tensioning is used, the resulting deviation forces – which are beneficial for the global load-bearing behaviour if an appropriate tendon layout is chosen, but cause local tensile (splitting) forces – need to be accounted for, which would also require transversal reinforcement. For both longitudinal reinforcement strategies, the layering of the concrete seemed to have no impact on the overall structural behaviour.

Cables, as well as fibres, can be used as interlayer shear reinforcement for layered digital fabrication processes. The results showed that, in both cases, the shear resistance could be increased significantly compared to the samples with no shear reinforcement. While cables showed a higher efficiency, fibres resulted in closer and thinner cracks. The bond in the interlayer is crucial when inserting reinforcement in the interlayers. For cables, this means that the cables should be fully anchored. This can be achieved by changing the direction of the cable or by providing adequate anchorage length. For cables, this bonding issue can be seen as a global issue, while for fibres, it is more of a local problem.

Both shear reinforcements were placed manually during the production of the samples. While the automation of cable placement also for large scale application has already been addressed [18], the automation of the fibre placement still remains a considerable challenge.

Furthermore, it needs to be mentioned that all beams of this study did fail in a brittle manner and did not achieve a sufficiently ductile behaviour in order to conduct a design according to the theory of plasticity. Ensuring ductile failure mechanism in digitally fabricated reinforced concrete structures requires future research efforts.

Acknowledgements

The authors gratefully acknowledge the students Jonathan Ensslin, Moritz Studer, Jean-Luc Imhof and Vanessa Studer for their valuable support during the production, preparation and testing of beams. The authors would also like to express their gratitude to the technical teams of the 'Structures Lab', the 'Robotic Fabrication Lab' and the 'Concrete Lab' at ETH Zurich and also to the Swiss National Science Foundation, which partially funded this work within the National Centre for Competence in Research in Digital Fabrication (project number 51NF40-141853).

References

[1] Wangler, T., Roussel, N., Bos, F.P., Salet, T.A.M., et al., Digital Concrete: A Review. *Cem. Concr. Res.* 2019, *123*, 105780.

[2] Asprone, D., Menna, C., Bos, F.P., Salet, T.A.M., et al., Rethinking reinforcement for digital fabrication with concrete. *Cem. Concr. Res.* 2018, *112*, 111–121.

[3] Gebhard, L., Mata-Falcón, J., Markić, T., Kaufmann, W., Aligned interlayer fibre reinforcement for digital fabrication with concrete, in: *RILEM-Fib X International Symposium on Fibre Reinforced Concrete, BEFIB2020 (Accepted)*, Valencia 2020.

[4] Gebhard, L., Mata-Falcón, J., Anton, A., Burger, J., et al., Aligned interlayer fibre reinforcement and post-tensioning as a reinforcement strategy for digital fabrication, in: *Digital Concrete 2020 (Accepted)*, Springer International Publishing, Eindhoven 2020.

[5] Bos, F.P., Ahmed, Z.Y., Jutinov, E.R., Salet, T.A., Experimental Exploration of Metal Cable as Reinforcement in 3D Printed Concrete. *Materials* 2017, *10*, 1314.

[6] Salet, T.A., Bos, F.P., Wolfs, R.J., Ahmed, Z.Y., 3D concrete printing–a structural engineering perspective, in: *High Tech Concrete: Where Technology and Engineering Meet*, Springer Cham, 2018.

[7] Bos, F., Wolfs, R., Ahmed, Z., Salet, T., Large Scale Testing of Digitally Fabricated Concrete (DFC) Elements, in: Wangler, T., Flatt, R.J. (Eds.), *First RILEM International Conference on Concrete and Digital Fabrication – Digital Concrete 2018*, Springer International Publishing, 2019, pp. 129–147.

[8] Debrunner Acifer AG Bewehrungen, Bartec Schraubenverbindungen Dokumentaiton. 2018.

[9] Jakob AG, Jakob Rope Systems Catalogue Hoisting Lifting C2. 2019.

[10] Bekaert, Dramix® 3D technical documents. *Bekaert* n.d.

[11] Gosselin, C., Duballet, R., Roux, Ph., Gaudillière, N., et al., Large-scale 3D printing of ultra-high performance concrete – a new processing route for architects and builders. *Mater. Des.* 2016, *100*, 102–109.

[12] Anton, A., Bedarf, P., Yoo, A., Reiter, L., et al., Concrete Choreography : Prefabrication of 3D Printed Columns, in: Burry, J., Sabin, J., Sheil, B., Skavara, M. (Eds.), *Fabricate Making Resilient Architecture*, UCL Press, 2020.

[13] Correlated Solutions, VIC 3D Software, Reference Manual v7. 2014.

[14] Haefliger, S., Mata-Falcón, J., Kaufmann, W., Application of distributed optical measurements to structural concrete experiments, in: *SMAR 2017 Proceedings*, ETH Zurich, 2017, p. 159.

[15] Mata-Falcón, J., Haefliger, S., Lee, M., Galkovski, T., et al., Combined application of distributed fibre optical and digital image correlation measurements to structural concrete experiments. *Eng. Struct. J.* 2020, *submitted for publication in 2020*.

[16] Gehri, N., Mata-Falcón, J., Kaufmann, W., Automated Crack Detection and Measurement based on Digital Image Correlation. *Constr. Build. Mater.* 2020, *submitted for publication in 2020*.

[17] Leonhardt, F., Walther, R., Schubversuche an einfeldrigen Stahlbetonbalken mit und ohne Schubbewehrung zur Ermittlung der Schubtragfähigkeit und der oberen Schubspannungsgrenze, Deutscher Ausschuss für Stahlbeton, Berlin 1962.

[18] Salet, T.A.M., Ahmed, Z.Y., Bos, F.P., Laagland, H.L.M., Design of a 3D printed concrete bridge by testing. *Virtual Phys. Prototyp.* 2018, *13*, 222–236.